Fibroblast Electrical Remodeling in Heart Failure and Potential Effects on Atrial Fibrillation

Martin Aguilar, MD Xiao Yan Qi, PhD Hai Huang, PhD Philippe Comtois, PhD
Stanley Nattel, MD

SUPPLEMENTAL MATERIALS

SUPPLEMENTAL FIGURES

Supplemental Figure 1

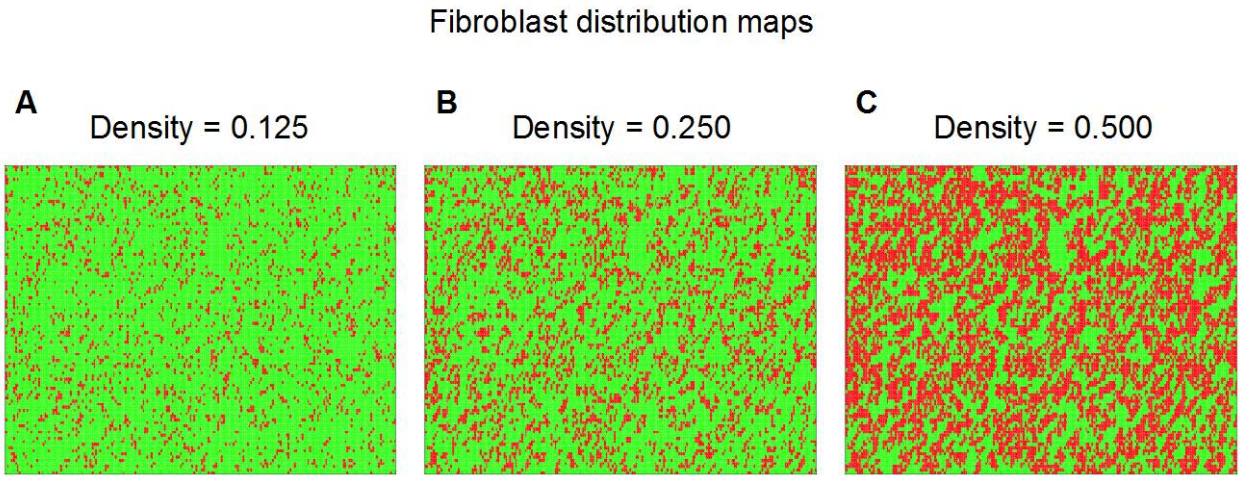

Supplemental Figure 1. Fibroblast distribution maps. Three different fibroblast distributions were investigated; low, medium and high densities corresponding to 12.5%, 25% and 50% of cardiomyocytes coupled to 2 fibroblasts. The red patches represent areas of fibrosis.

Supplemental Figure 2

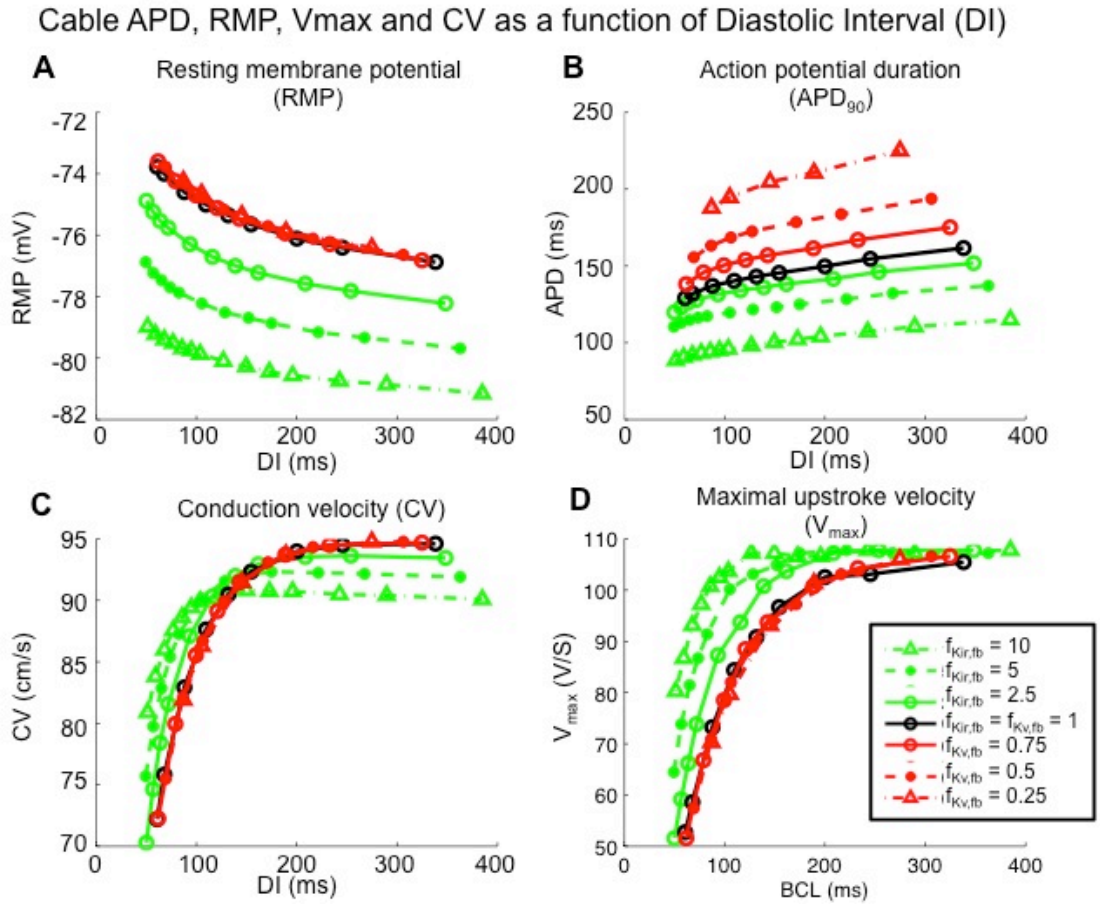

Supplementary Figure 2. Effect of progressive $I_{Kv,fb}$ downregulation (red curves) and $I_{Kir,fb}$ upregulation (green curves) on the cardiomyocyte resting membrane potential (RMP), action potential duration (APD_{90}), conduction velocity (CV) and maximal upstroke velocity (V_{max}) as a function of the diastolic interval (DI) for a 10-cm cable of cardiomyocytes with 2 fibroblasts per cardiomyocyte with G_{gap} of 3 nS. The control curve in black is for $f_{Kv,fb} = f_{Kir,fb} = 1$. $I_{Kv,fb}$ downregulation had a small depolarizing effect on the RMP, prolonged APD_{90}, with negligible effect on CV. $I_{Kir,fb}$ upregulations had the opposite effect; it significantly hyperpolarized RMP, shortened APD_{90} and preserved CV and 1:1 conduction at progressively shorter DIs with increasing $f_{Kir,fb}$.

Supplementary Figure 3

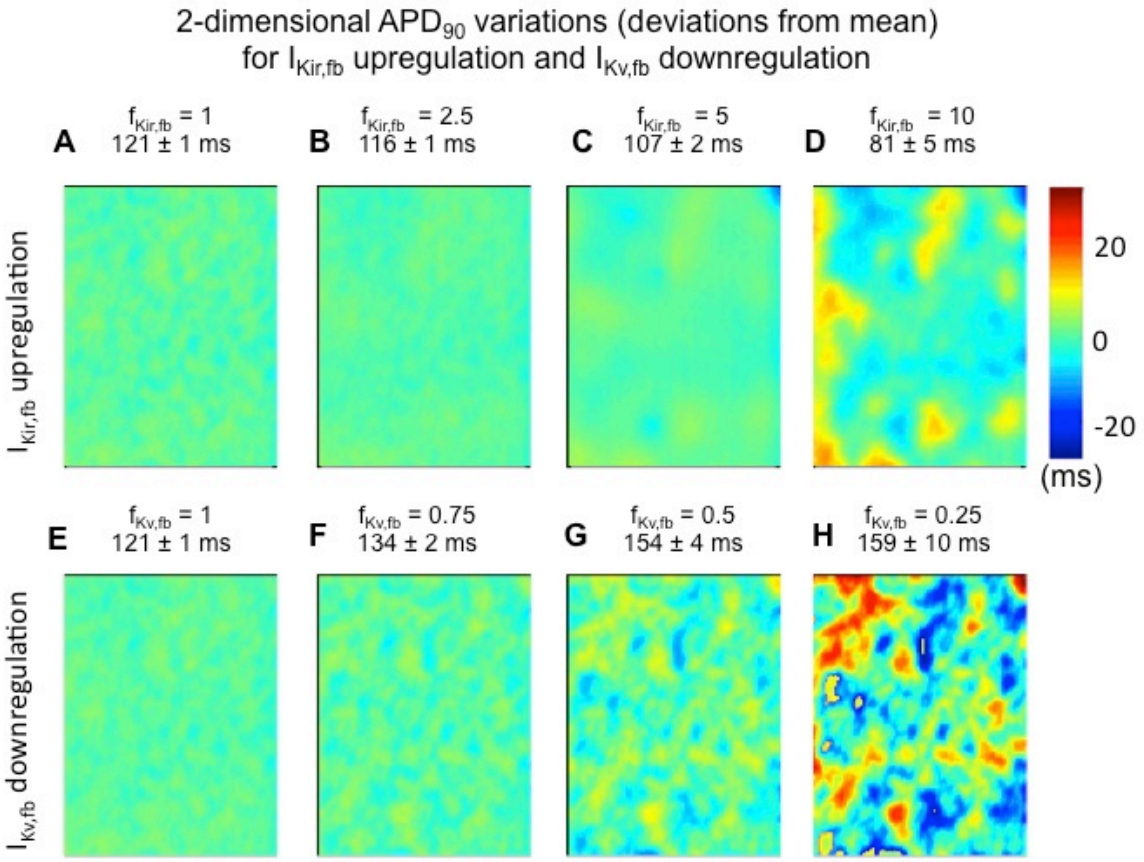

Supplementary Figure 3. Distribution of APD_{90}-deviations from mean-values over a 2-dimensional sheet of cardiomyocytes with patchy fibrosis (2 fibroblasts per cardiomyocyte with a G_{gap} of 3 nS) in the 2-dimensional model for progressive $I_{Kir,fb}$ upregulation (top row, panels A-D) and $I_{Kv,fb}$ downregulation (bottom row, panels E-H). APD_{90} dispersion, as indicated by the standard deviation, increases with both $I_{Kir,fb}$ upregulation and $I_{Kv,fb}$ dowregulation from <1% to 6%. Values above each panel are mean±standard deviation APD_{90} across the substrate.

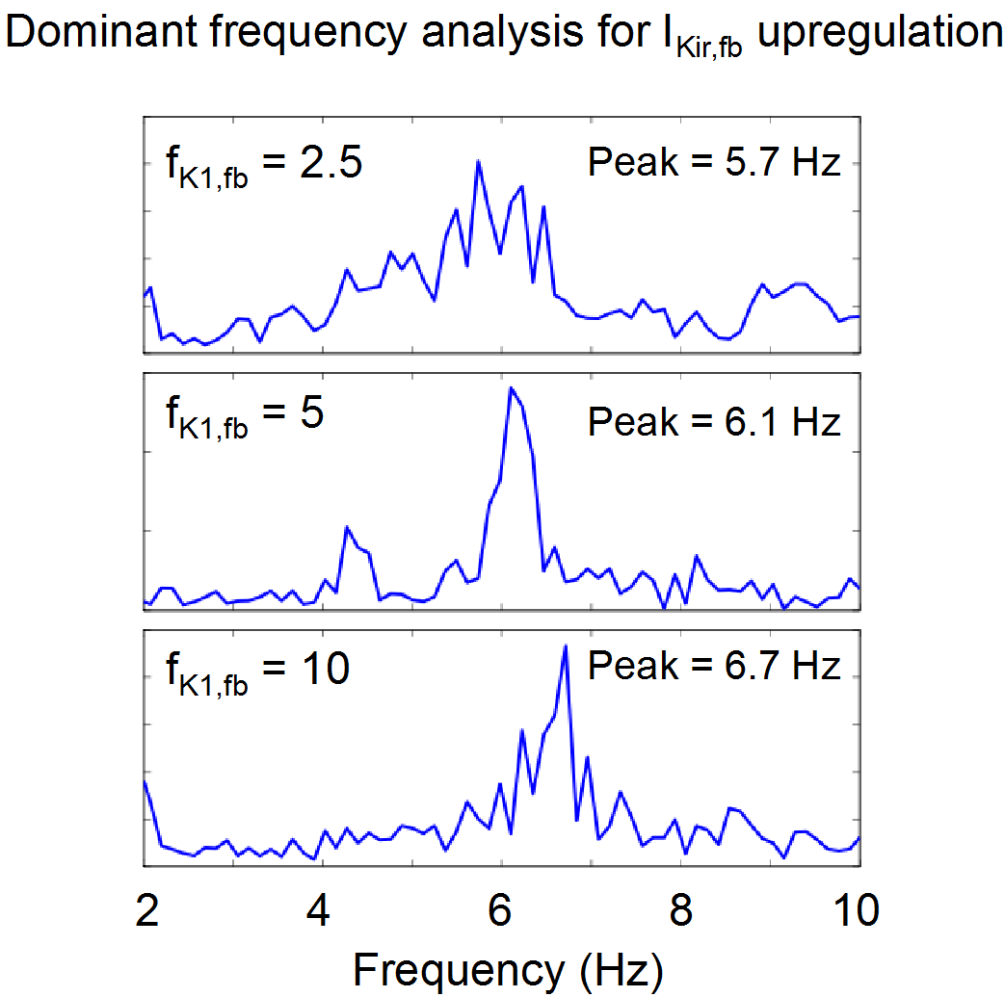

Supplemental Figure 4. Power spectrum analysis for $f_{Kir,fb}$ = {2.5, 5, 10}. $I_{Kir,fb}$ upregulation progressively increased the spiral-wave dominant frequency from 5.7 to 6.7 Hz. For $f_{Kir,fb}$ = 1, reentry was non-sustained, precluding precise computation of the dominant frequency, but it was estimated at 4.6 Hz.

Supplemental Figure 5

Spiral wave dynamics with progressive $I_{Kv,fb}$ downregulation

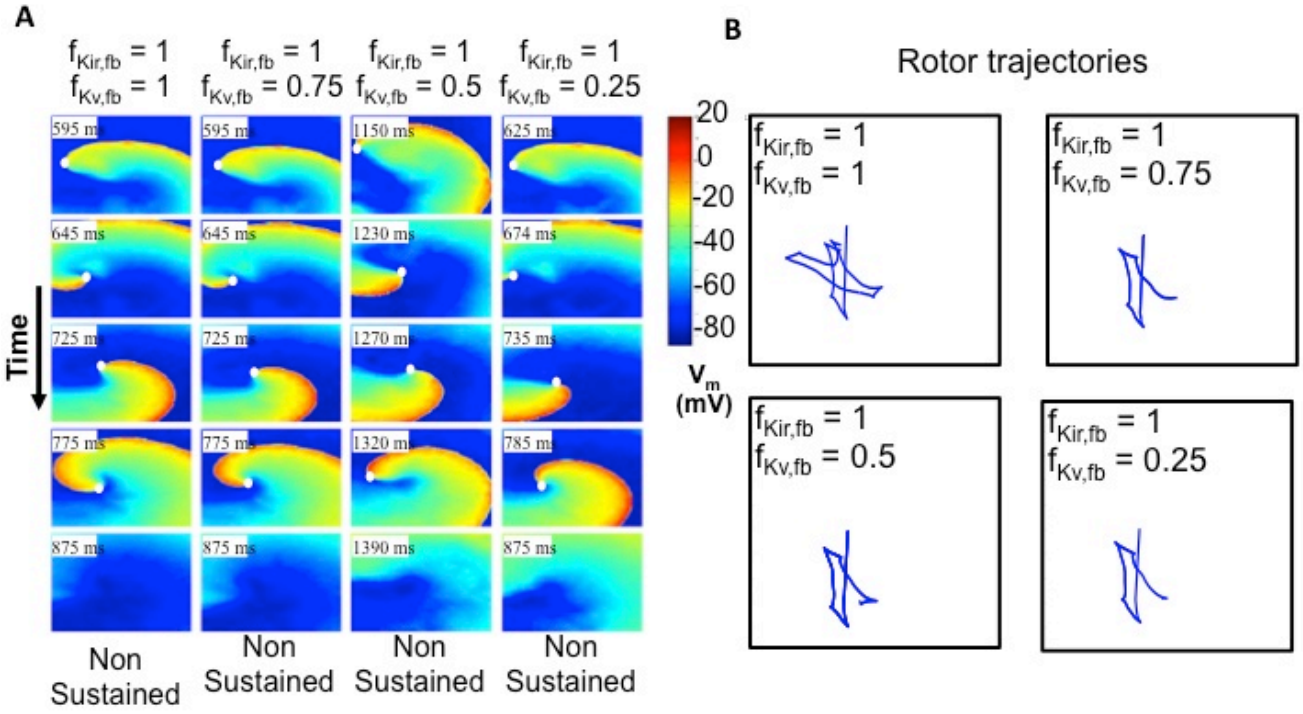

Supplementary Figure 5. (A) Spiral-wave dynamics over time for progressive $I_{Kv,fb}$ downregulation for fixed $I_{Kir,fb}$. White dots identify the rotor-tip phase-singularities. In the control condition ($f_{Kir,fb}$ = $f_{Kv,fb}$ = 1), the phase-singularity drifts and extinguishes on a boundary. As $I_{Kv,fb}$ is downregulated ($f_{Kv,fb}$ = 0.5 and 0.25), the wavefront fails to depolarize surrounding cardiomyocytes, leading to propagation failure and termination. (B) Rotor trajectory for the corresponding simulations in (A). Qualitatively similar trajectories were observed.

Supplemental Figure 6

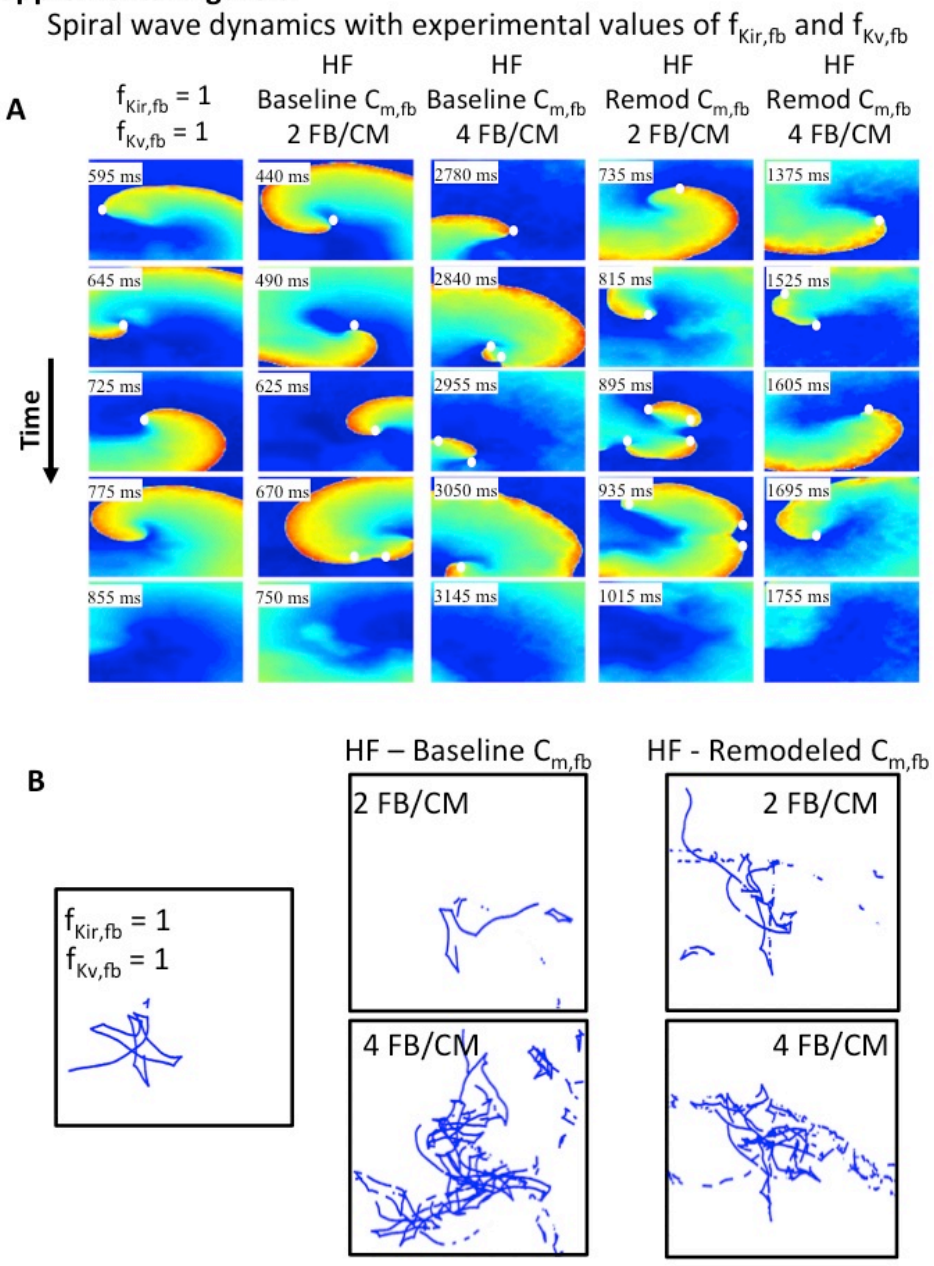

Supplementary Figure 6. Spiral-wave dynamics for the control ($f_{Kir,fb}$ = $f_{Kv,fb}$ = 1) and HF-induced fibroblast ionic and capacitance remodeling ($f_{Kir,fb}$ = 1.79 and $f_{Kv,fb}$ = 0.56; $C_{m,fb}$ remodeled = 1.67×$C_{m,fb}$ baseline) using moderate fibroblast density distribution (0.250) with 2 and 4 fibroblasts/cardiomyocyte. HF with 2 fibroblasts/cardiomyocyte led to non-sustained reentry, similar to the control case; however, rotor trajectory complexity was qualitatively increased with remodeled $C_{m,fb}$. Using 4 fibroblasts/cardiomyocte also led to non-sustained reentry; however, the time to termination was longer compared to control and HF with 2 fibroblasts/cardiomyocyte for both $C_{m,fb}$ settings. (B) Respective rotor trajectories. All cases were non-sustained, but HF with 4 fibroblasts/cardiomyocyte displayed more complex and longer-lasting dynamics.

Supplemental Figure 7

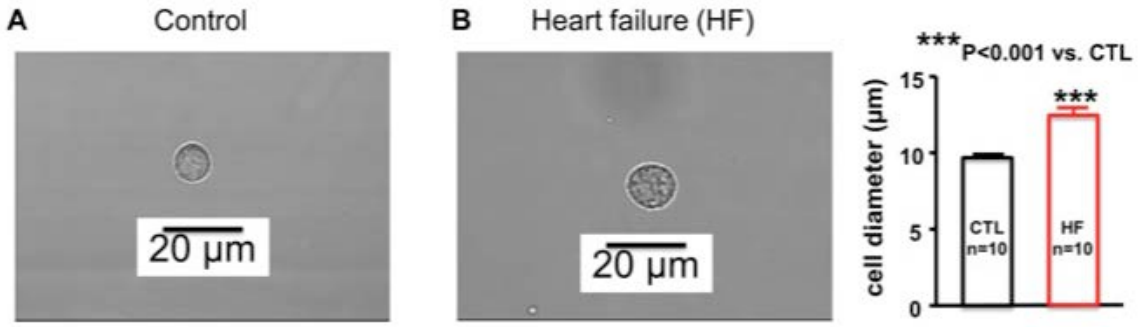

Supplemental Figure 7. Size difference between a control (A) and heart failure (B) fibroblast, along with mean cell diameter values for 10 cells of each type. Heart failure increased fibroblast size accounting, at least in part, for the increase in the membrane capacitance in heart failure compared to control.

Supplemental Figure 8

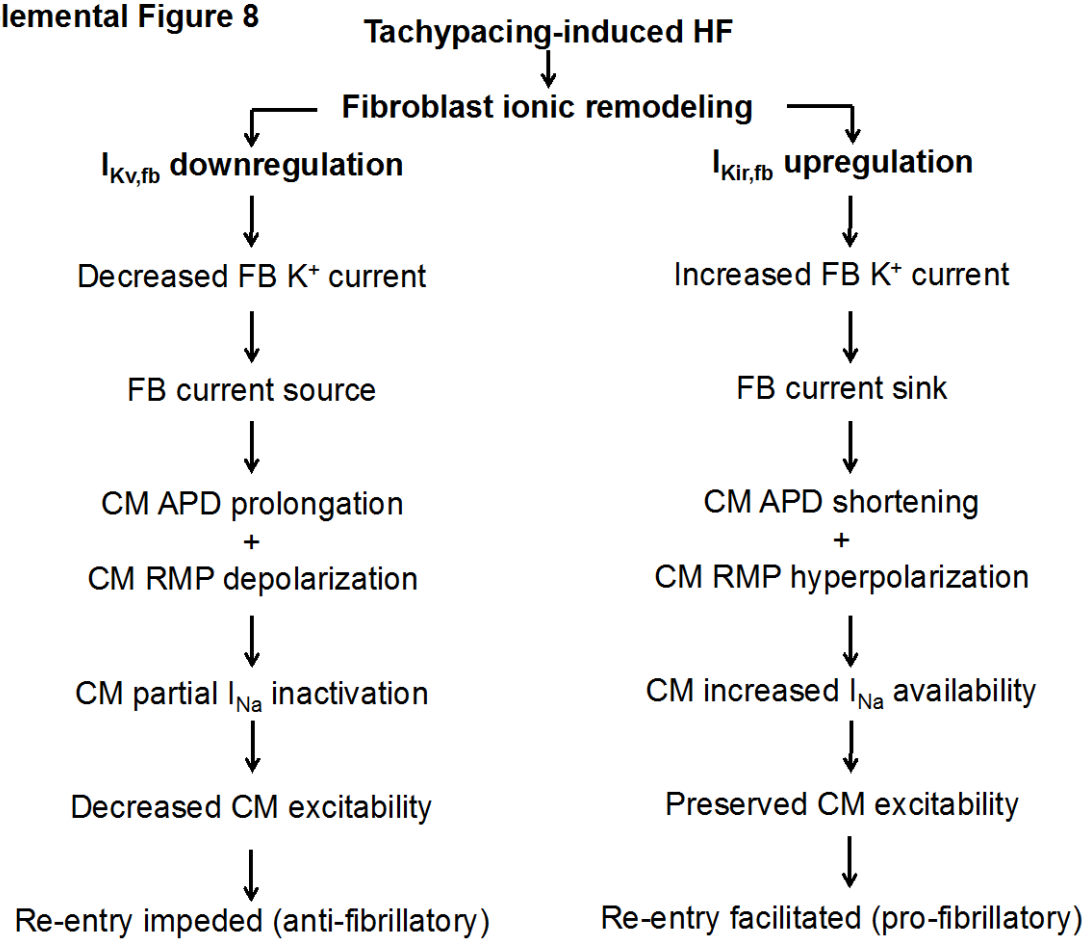

Supplementary Figure 8. Summary of electrophysiological effects observed for fibroblast electrical remodeling and consequences for atrial arrhythmogenesis. $I_{Kv,fb}$ downregulation in tachypacing-induced HF leads to decreased fibroblast (FB) repolarizing current, thus making it a source of depolarizing current for the cardiomyocyte (CM). This effect prolongs cardiomyocyte APD and depolarizes RMP, thus inducing I_{Na} inactivation, reduced V_{max}, CV and cardiomyocyte excitability and impeding reentry (anti-fibrillatory effect). $I_{Kir,fb}$ was upregulated in tachypacing-induced HF, leading to increased fibroblast repolarizing current and making the fibroblast a current sink for the myocyte. This effect shortened cardiomyocyte APD and hyperpolarizing RMP, increasing I_{Na} availability, maintaining V_{max}, CV and cardiomyocyte excitability at high activation frequencies, thereby facilitating reentry (pro-fibrillatory effect).

Supplemental Figure 9 Spiral wave dynamics with and without cardiomyocyte and fibroblast remodeling

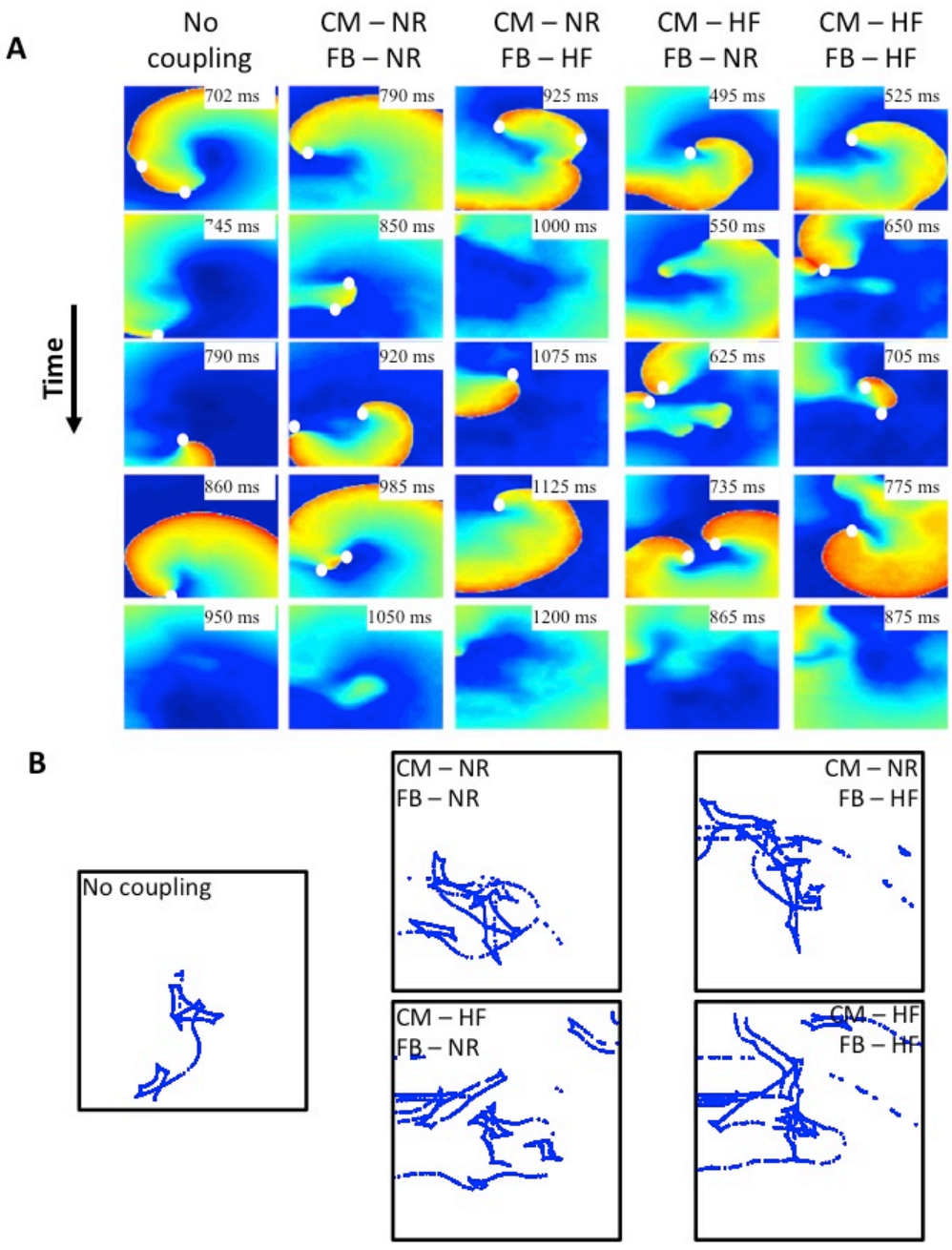

Supplemental Figure 9 Effect of the experimentally observed cardiomyocyte and fibroblast ionic and capacitance remodeling on reentry dynamics (A) and rotor trajectories (B). Two-dimensional reentry dynamics with and without cardiomyocyte ionic and capacitance remodeling were qualitatively similar, although termination was slightly faster with the remodeled cardiomyocyte. Fibroblast remodeling tended to prolong the duration of reentry but did not have a significant qualitative effect.

Supplemental Figure 10

2D time to termination for control, proarrhythmic and antiarrhythmic conditions for variable N_{fb}, G_{gap}, and $C_{m,fb}$

A

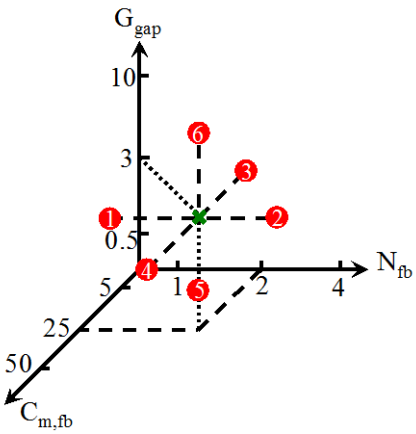

B

#	N_{fb}	G_{gap} (nS)	$C_{m,fb}$ (pF)	a: $f_{Kir,fb}$=1, $f_{Kv,fb}$=1	b: $f_{Kir,fb}$=10, $f_{Kv,fb}$=1	c: $f_{Kir,fb}$=1, $f_{Kv,fb}$=0.25
				Time to termination (ms)		
1	1	3	25	943	1439	957
2	4	3	25	451	S	469
3	2	3	5	938	1096	948
4	2	3	50	441	S	464
5	2	0.5	25	933	S	953
6	2	10	25	430	S	440
CTL	2	3	25	1143	S	437

Supplemental Figure 10. Effect of varying the number of fibroblasts per cardiomyocyte (N_{fb}), gap junction conductance (G_{gap}) and fibroblast capacitance ($C_{m,fb}$) on spiral-wave dynamics for non-remodeled (a), proarrhythmic (b) and antiarrhythmic (c) conditions. (A) Parameter-space of N_{fb}, G_{gap} and $C_{m,fb}$; the green X represents the default parameter-set used for all simulations in the paper, while the red dots indicate the variations indicated by the red numbers in the table in B. (B) Decreasing N_{fb} attenuated the proarrhythmic effect of $I_{Kir,fb}$-upregulation (#1b vs. CTLb) and antiarrhythmic effect of $I_{Kv,fb}$-downregulation (#1c vs. CTLc). Increasing the N_{fb} (#2) did not have clear effects. Reducing fibroblast-capacitance ($C_{m,fb}$) greatly attenuated effects of fibroblast ion-channel remodeling (#3b and #3c barely changed vs. #3a). Increasing $C_{m,fb}$ (#4) reduced baseline AF-persistence (#4a vs. CTLa) but did not appreciably alter persistence with remodeling (#4b and #4c vs. CTLb and CTLc respectively). Reducing G_{gap} reduced baseline rotor-persistence (#5a vs. CTLa) and virtually eliminated the effects of $I_{Kv,fb}$-downregulation (#5c barely changed vs. #5a), but AF remained sustained with $I_{Kir,fb}$-upregulation (#5b). Increasing G_{gap} did not appreciably alter the effects of ionic remodeling (#6b and #6c vs. CTLb and CTLc respectively).

Supplemental Table 1: Experimental single cell APD_{90} and ERP and matched simulated single cell APD_{90}.

	CTL (ms)	HF (ms)
Experimental (Li et al., *Circulation.* 101:2631-2638)		
APD_{90} at 3Hz	138	145
Simulated		
APD_{90} at 3Hz	139	148

Supplemental Table 2: Experimental and simulated ERP for control and remodeled conditions with and without fibroblasts.

	Experimental		Simulated					
	CTL	HF	CM CTL	CM HF	CM CTL FB CTL	CM CTL FB HF	CM HF FB CTL	CM HF FB HF
FB/CM	-	-	0	0	2	2	2	2
ERP (ms)	131	149	144	188	164	171	189	196

We implemented the HF-induced cardiomyocyte ionic and capacitance remodeling as described by Li et al. (*Circulation* (2000) 101:2631-2638) into the single-cell model and adjusted the mathematical model to match experimental APD_{90} (Supplemental Table 1). We then used these single-cell parameters in the 2D-model to compare the experimental control (CTL) and HF-remodeled (HF) ERP to the ERP computed in the model for the CTL and HF cardiomyocyte with and without fibroblasts. The mathematical model was able to qualitatively reproduce the experimentally observed ERP prolongation in HF. Introducing fibroblasts had either no effect on ERP (CM-HF+CTL fibroblast currents/capacitance versus CM-HF) or prolonged ERP (CM-HF+HF fibroblast currents/capacitance versus CM-HF).